Dalton Transactions

Accepted Manuscript

ROYAL SOCIETY OF CHEMISTRY

www.rsc.org/dalton

Cite this: DOI: 10.1039/c0xx00000x

www.rsc.org/xxxxxx

PAPER

Syntheses, Structures and Photocatalytic Properties of Five New Praseodymium–Antimony Oxochlorides: From Discrete Cluster to 3D Inorganic–Organic Hybrid Racemic Compound

Guo–Dong Zou,[a,b] Ze–Ping Wang,[a,c] Ying Song,[a,b] Bing Hu[a] and Xiao–Ying Huang*[a]

Received (in XXX, XXX) Xth XXXXXXXXX 20XX, Accepted Xth XXXXXXXXX 20XX
DOI: 10.1039/b000000x

Five novel praseodymium–antimony oxochloride (Pr–Sb–O–Cl) cluster–based compounds, namely, (2-MepyH)$_2$[Fe(1,10-phen)$_3$]$_2$[Pr$_4$Sb$_{12}$O$_{18}$Cl$_{14.6}$(OH)$_{2.4}$(Hsal)]·H$_2$O (**1**), (2-MepyH)$_2$[Fe(1,10-phen)$_3$]$_4${[Pr$_4$Sb$_{12}$O$_{18}$Cl$_{13.5}$(OH)$_{0.5}$](bcpb)$_2$[Pr$_4$Sb$_{12}$O$_{18}$Cl$_{13.5}$(OH)$_{0.5}$]}·42H$_2$O (**2**), (3-MepyH)$_2$[Fe(1,10-phen)$_3$]{[Pr$_4$Sb$_{12}$O$_{18}$Cl$_{13}$(H$_2$O)$_2$](bcpb)}·2(3-Mepy)·3H$_2$O (**3**), [Fe(1,10-phen)$_3$]$_2${[Pr$_4$Sb$_{12}$O$_{18}$Cl$_{10}$(H$_2$O)$_2$](bcpb)$_2$}·3(3-Mepy)·13H$_2$O (**4**), and (2-MepyH)$_6$[Fe(1,10-phen)$_3$]$_{10}${[Pr$_4$Sb$_{12}$O$_{18}$Cl$_{13}$(OH)$_2$]$_2$[Pr$_4$Sb$_{12}$O$_{18}$Cl$_9$][Pr$_4$Sb$_{12}$O$_{18}$Cl$_9$(OH)$_2$]$_2$(Hpdc)$_{10}$(pdc)$_2$}·110H$_2$O (**5**) (2-Mepy = 2-methylpyridine, 3-Mepy = 3-methylpyridine, 1,10-phen = 1,10-phenanthroline, H$_2$sal = salicylic acid, H$_3$bcpb = 3,5-bis(4-carboxyphenoxy)benzoic acid, H$_3$pdc = 3,5-pyrazoledicarboxylic acid) have been solvothermally synthesized and structurally characterized. Compound **1** is the first zero-dimensional (0D) Pr–Sb–O–Cl cluster decorated by organic ligand. Compounds **2**–**4** are constructed from the same H$_3$bcpb ligands but adopt different structures: **2** represents a rare example of one-dimensional (1D) nanotubular structure based on high–nuclearity clusters; **3** exhibits two-dimensional (2D) mono-layered structure, in which left-handed and right-handed helical chains are alternately arranged; while **4** features a double-layered structure with an unprecedented (3,3,6)-connected 3-nodal topological net. Compound **5** is a unique three-dimensional (3D) 2-fold interpenetrating racemic compound, simultaneously containing three kinds of Pr–Sb–O–Cl–pdc clusters. UV–light photocatalytic H$_2$ evolution activity was observed for compound **3** with Pt as a co-catalyst and MeOH as a sacrificial electron donor. In addition, the magnetic properties of compounds **1** and **5** are also studied.

Introduction

The rational design and synthesis of inorganic–organic hybrid materials, based on high–nuclearity clusters acting as inorganic polydentate secondary building units (SBU), are of great interest not only for their intriguing variety of architectures and fascinating topologies but also for their potential applications in catalysis, magnetism, photochemistry, medicine and nanoscience.[1] Amongst them, the polyoxometalates (POMs) as a large family of well–defined transition–metal–oxygen clusters have been used to construct novel extended frameworks by means of different organic linkers.[2] Other structural types such as metal–chalcogenide–cluster–based hybrid frameworks have also been reported.[3] Following our recent report of an unprecedented high–nuclearity rare–earth/main–group–metal oxochloride cluster, namely [Pr$_4$Sb$_{12}$O$_{18}$Cl$_{17}$]$^{5-}$, up to now we have successfully obtained a series of inorganic–organic hybrid compounds with structures ranging from one–dimensional (1D) chains to three–dimensional (3D) networks by utilizing the single oxochloride cluster as SBU and diverse bifunctional organic ligands as linkers.[4] Next, it is hoped to design more diversiform oxochloride cluster SBUs and appropriately choose well-designed organic ligands as linkers or terminal groups to obtain novel hybrid structures, which may exhibit unique physical or chemical properties.

Since the first discovery of carbon nanotubes (CNTs) by Iijima in 1991,[5] nanotubular structures, including inorganic nanotubes containing elements other than carbon (e.g., B, N, S and Si)[6] and organic nanotubes (e.g., cyclic peptides, lipids and cyclodextrins),[7] have been successfully developed. These studies were motivated by their intriguing architectures which include uniform and fixed internal diameters, and more importantly, their potential applications in ion exchange, catalysts, molecular capillaries, sieves, and biological models.[8] Although abundant metal–organic frameworks (MOFs) with open channels have been synthesized in the past decades,[9] it is surprising that significantly less effort has been directed to the preparation of metal–organic nanotubes (MONTs).[10] Furthermore, the discrete MONT structures are not common,[11] in particular those constructed from high–nuclearity cluster and multifunctional organic ligand.[3b] Instead of forming a discrete 1D cylindrical structure, high–nuclearity clusters with multi-metal coordination sites are easier to be assembled into high-dimensional frameworks through further interconnection of them by the

multidentate ligands. Therefore, it is a particularly interesting and greatly challenging subject to construct discrete nanotubular structure based on high–nuclearity clusters.

Photocatalytic water splitting with solar energy provides a promising way to produce hydrogen as a source of clean and renewable energy. Since the discovery of H_2 production by water splitting on titanium dioxide electrodes under UV irradiation in 1972,[12] a significant process has been achieved on photocatalytic hydrogen generation through water reduction.[13] Various kinds of homogeneous and heterogeneous photocatalytic systems have been explored in the past few decades, based mostly on dense structures such as binary and ternary oxides.[14] By contrast, the applications of other structure types such as high–nuclearity cluster–based compounds in this field are still in its infancy. The POMs that possess diverse compositions and tunable electronic band structures have been found to exhibit good photocatalytic activity for H_2 evolution.[15] Recently our group also reported a 3D hybrid network based on $[Pr_4Sb_{12}O_{18}Cl_{17}]^{5-}$ cluster units that showed benign photocatalytic activity for H_2 evolution.[4c] The above results suggest that high–nuclearity cluster–based compounds would be promising candidates for photocatalysis.

As part of our ongoing efforts on the exploration of novel Pr–Sb–O–Cl cluster–based hybrid materials, herein we report the syntheses, structures and property studies of five compounds, namely $(2\text{-MepyH})_2[Fe(1,10\text{-phen})_3]_2[Pr_4Sb_{12}O_{18}Cl_{14.6}(OH)_{2.4}(Hsal)]\cdot H_2O$ (**1**), $(2\text{-MepyH})_2[Fe(1,10\text{-phen})_3]_4\{[Pr_4Sb_{12}O_{18}Cl_{13.5}(OH)_{0.5}](bcpb)_2[Pr_4Sb_{12}O_{18}Cl_{13.5}(OH)_{0.5}]\}\cdot 42H_2O$ (**2**), $(3\text{-MepyH})_2[Fe(1,10\text{-phen})_3]\{[Pr_4Sb_{12}O_{18}Cl_{13}(H_2O)_2](bcpb)\}\cdot 2(3\text{-Mepy})\cdot 3H_2O$ (**3**), $[Fe(1,10\text{-phen})_3]_2\{[Pr_4Sb_{12}O_{18}Cl_{10}(H_2O)_2](bcpb)_2\}\cdot 3(3\text{-Mepy})\cdot 13H_2O$ (**4**), $(2\text{-MepyH})_6[Fe(1,10\text{-phen})_3]_{10}\{[Pr_4Sb_{12}O_{18}Cl_{13}(OH)_2]_2[Pr_4Sb_{12}O_{18}Cl_9][Pr_4Sb_{12}O_{18}Cl_9(OH)_2]_2(Hpdc)_{10}(pdc)_2\}\cdot 110H_2O$ (**5**) (2-Mepy = 2-methylpyridine, 3-Mepy = 3-methylpyridine, 1,10-phen = 1,10-phenanthroline, H_2sal = salicylic acid, H_3bcpb = 3,5-bis(4-carboxyphenoxy)benzoic acid, H_3pdc = 3,5-pyrazoledicarboxylic acid). In addition, the photocatalytic H_2-evolution activity of compound **3** and the magnetic properties of compounds **1** and **5** have been studied in detail.

Experimental

Materials and physical measurements

All chemicals were commercially purchased and used without further purification. Powder X-ray diffraction (PXRD) patterns were recorded on a Rigaku Miniflex II diffractometer using Cu*Kα* radiation. C, H and N analyses were performed on a German Elementary Vario EL III instrument. Thermogravimetric analyses (TGA) were carried out on a NETZSCH STA 449F3 unit at a heating rate of 5 °C/min under a nitrogen atmosphere. Thermogravimetric analyses–mass spectra (TGA–MS) were carried out on a NETZSCH STA449C–QMS 403C unit at a heating rate of 10 °C/min under a nitrogen atmosphere. Optical diffuse reflectance spectra were measured at room temperature with a Varian Cary 500 Scan UV-visible system. A $BaSO_4$ plate was used as a standard (100% reflectance). The variable–temperature magnetic susceptibility (2–300 K) was measured with a Quantum Design MPMS–XL SQUID magnetometer under an applied field of 1000 Oe with the crystalline powder samples kept in a capsule for weighing.

Preparation of compounds 1−5

Synthesis of compound 1: A mixture of $PrCl_3\cdot 6H_2O$ (0.178 g, 0.5 mmol), $SbCl_3$ (0.342 g, 1.5 mmol), H_2sal (0.069 g, 0.5 mmol), $FeCl_3\cdot 6H_2O$ (0.135 g, 0.5 mmol), 1,10-phen·H_2O (0.297 g, 1.5 mmol) and NaOH (0.040 g, 1 mmol) in 2-Mepy/H_2O (5 mL/1.5 mL) was sealed in a 28 mL Teflon-lined stainless-steel autoclave at 150 °C for 3 days, then cooled down to room temperature. Dark red block crystals (manually selected, yield: 0.040 g, 7.3% based on Pr) were obtained. Elemental analysis: calcd (%) for $C_{91}H_{73.4}N_{14}O_{24.4}Cl_{14.6}Fe_2Sb_{12}Pr_4$ (1): C: 24.80; H: 1.68; N: 4.45; found: C: 24.47; H: 1.73; N: 4.34.

Synthesis of compound 2: A mixture of $PrCl_3\cdot 6H_2O$ (0.178 g, 0.5 mmol), $SbCl_3$ (0.342 g, 1.5 mmol), H_3bcpb (0.197 g, 0.5 mmol), $FeCl_3\cdot 6H_2O$ (0.135 g, 0.5 mmol), 1,10-phen·H_2O (0.297 g, 1.5 mmol) and NaOH (0.060 g, 1.5 mmol) in 2-Mepy/H_2O (10 mL/1.5 mL) was sealed in a 28 mL Teflon-lined stainless-steel autoclave at 160 °C for 3 days, then cooled down to room temperature. Dark red strip crystals (manually selected, yield: 0.020 g, 3.3% based on Pr) were obtained. Elemental analysis: calcd (%) for $C_{198}H_{219}N_{26}O_{95}Cl_{27}Fe_4Sb_{24}Pr_8$ (**2**): C: 24.48; H: 2.27; N: 3.75; found: C: 24.20; H: 1.97; N: 3.86.

Syntheses of compounds 3 and 4: A mixture of $PrCl_3\cdot 6H_2O$ (0.178 g, 0.5 mmol), $SbCl_3$ (0.342 g, 1.5 mmol), H_3bcpb (0.197 g, 0.5 mmol), $FeCl_3\cdot 6H_2O$ (0.135 g, 0.5 mmol), 1,10-phen·H_2O (0.297 g, 1.5 mmol) and NaOH (0.060 g, 1.5 mmol) in 3-Mepy/H_2O (5 mL/1.5 mL) was sealed in a 28 mL Teflon-lined stainless-steel autoclave at 150 °C for 3 days, then cooled down to room temperature. Red sheet crystals of compound **3** (manually selected, yield: 0.035 g, 6.7% based on Pr) and dark red sheet crystals of compound **4** (manually selected, yield: 0.040 g, 6.2% based on Pr) were obtained simultaneously. Elemental analysis: calcd (%) for $C_{81}H_{75}N_{10}O_{31}Cl_{13}FeSb_{12}Pr_4$ (**3**): C: 23.02; H: 1.79; N: 3.31; found: C: 22.65; H: 1.83; N: 3.38. Elemental analysis: calcd (%) for $C_{132}H_{121}N_{15}O_{49}Cl_{10}Fe_2Sb_{12}Pr_4$ (**4**): C: 30.53; H: 2.35; N: 4.05; found: C: 30.50; H: 2.23; N: 4.15.

Synthesis of compound 5: A mixture of $PrCl_3\cdot 6H_2O$ (0.178 g, 0.5 mmol), $SbCl_3$ (0.342 g, 1.5 mmol), H_3pdc·H_2O (0.087 g, 0.5 mmol), $FeCl_3\cdot 6H_2O$ (0.135 g, 0.5 mmol), 1,10-phen·H_2O (0.297 g, 1.5 mmol) and NaOH (0.040 g, 1 mmol) in 2-Mepy/H_2O (5 mL/1.5 mL) was sealed in a 28 mL Teflon-lined stainless-steel autoclave at 140 °C for 4 days, then cooled down to room temperature. Dark red prismatic crystals (manually selected, yield: 0.050 g, 8.4% based on Pr) were obtained. Elemental analysis: calcd (%) for $C_{456}H_{538}N_{90}O_{256}Cl_{53}Fe_{10}Sb_{60}Pr_{20}$ (**5**): C: 22.88; H: 2.27; N: 5.27; found: C: 22.66; H: 2.04; N: 5.42.

UV-light Photocatalytic Activity for Hydrogen Evolution

H_2 production was performed by dispersing 50 mg powdered compound **3** in an aqueous solution (100 mL) containing CH_3OH (10 vol%) as a sacrificial electron donor. 3 wt% Pt was loaded on the surface of the catalyst by the in situ photodeposition method using H_2PtCl_6. The photocatalytic reaction was carried out in a Pyrex top–irradiation–type reaction vessel connected to a glass closed gas system. The catalyst suspension was irradiated under a

300 W Xe lamp equipped with a UVREF filter. The temperature of the reaction solution was maintained at room temperature by the flow of cooling water during the reaction. The evolved gases were analyzed by gas chromatography equipped with a thermal conductive detector (TCD) and a TDX–01 column, using argon as the carrier gas.

X-ray Crystallography

The X-ray diffraction data were collected at room temperature on a Rigaku 724 CCD diffractometer for **1** and an Oxford Xcalibur Eos CCD diffractometer for **3** and **4**, respectively, with graphite-monochromated Mo*Kα* radiation (λ = 0.71073 Å); for structures **2** and **5**, the single-crystal diffraction data were collected on a SuperNova CCD diffractometer with graphite-monochromated Cu*Ka* radiation (λ = 1.54178 Å) at 100(2) K. The structures were solved by direct methods and refined by full–matrix least–squares on F^2 by using the SHELX–2013 program package.[16] Anisotropic thermal factors were assigned to most of the non-disordered non-hydrogen atoms except for a few 2-Mepy, 3-Mepy and water molecules showing severe disorder. The positions of the hydrogen atoms bonded to carbon and nitrogen were generated geometrically, assigned isotropic thermal parameters, and allowed to ride on their respective parent atoms before the final cycle of least–squares refinement. The details of crystallographic data for **1**–**5** are summarized in Table 1. In the five compounds, some constraints (FLAT, DFIX, SIMU, SADI and ISOR) were applied to 2-Mepy, 3-Mepy, 1,10-phen and H_3pdc to obtain the chemical–reasonable models and reasonable atomic displacement parameters. It was difficult to locate all the disordered guest water molecules according to the D–F maps for compounds **2** and **4**; therefore, finally only partial lattice water molecules were assigned and refined. The amount of the remaining water molecules per formula was calculated according to the EA and TGA analyses. For compound **5**, the final refinement was performed with modification of the structural factors for the electron densities of the disordered guest water molecules using the SQUEEZE routine of the PLATON software package.[17] A few large residual density peaks close to the metal atoms are present due to the smearing effect of the heavy metals which show no feature.

Notably, to obtain better refinement results for compounds **2** and **5** with high R_1 values, we have tried our best to collect single-crystal diffraction data sets several times for compound **2** (or **5**) with Cu*Ka* radiation at 100(2) K, by selecting different single crystals with good quality. Usually, the large structures like **2** and **5** (> 380 non-hydrogen atoms per asymmetric unit in either of them) are never easy structures. Some large structures documented also have high R_1 values.[18]

CCDCs 976937 (**1**), 976938 (**2**), 976939 (**3**), 976940 **(4)** and 976941 **(5)** contain the supplementary crystallographic data for this paper. The data can be obtained free of charge from The Cambridge Crystallographic Data Centre via www.ccdc.cam.ac.uk/data_request/cif.

Results and discussion

Synthesis

The solvothermal reactions of $PrCl_3{\cdot}6H_2O$, $SbCl_3$, carboxylate ligands, $FeCl_3{\cdot}6H_2O$, 1,10-phen$\cdot H_2O$ and NaOH resulted in the formation of compounds **1**–**5** under different reaction conditions. In our previous studies, a range of dicarboxylate ligands were selected to construct inorganic–organic hybrid frameworks. In order to gain a deeper insight into the influence of organic ligands on the coordination architectures and related properties, in this work we carried out the solvothermal reactions with three types of ligands involving mono-, di-, and tri-carboxylate ligands: H_2sal (for **1**), H_3bcpb (for **2**, **3** and **4**) and H_3pdc (for **5**). In the 2-Mepy/H_2O (v/v = 5:1.5) component solvent system, compounds **1**, **2** and **5** were prepared at different reaction temperatures; whereas a mixed phases of **3** and **4** with nearly equal yield were obtained simultaneously from the same reaction in the 3-Mepy/H_2O (v/v = 5:1.5) component solvent system.

Although we have successfully prepared 1D to 3D Pr–Sb–O–Cl cluster-based hybrid compounds to date,[4] the discrete structure constructed from the above cluster-based SBU and organic ligand has not been reported. Usage of the mono-carboxylate ligand H_2sal which usually acts as a terminal group to construct low-dimensional coordination compounds,[19] the zero-dimensional (0D) cluster-based compound **1** was successfully obtained.

H_3bcpb triangular flexible ligand (Scheme 1), in which the two carboxyphenoxy groups are connected to the other such group through two oxygen atoms, can adopt various conformations under different conditions, owing to their varied coordination modes and flexible molecular backbones. When they coordinate to metal ions/clusters, diverse structures and specific topologies can be formed.[20] By employing this flexible H_3bcpb ligand, compounds **2**–**4** exhibiting obvious structural differences were prepared. It is notable that the ligands take on five different coordination conformations in the three structures and are found wholly de-protonated. Compound **2** consists of discrete 1D nanotubular structure, while compounds **3** and **4** exhibit 2D mono- and double-layered structures, respectively.

Besides the O-donor ligand, a further exploration of the influence of multifunctional ligands simultaneously containing N- and O-donors on the inorganic–organic self-assembling process is attempted. In this work, the selection of H_3pdc ligand is based on the following considerations: (i) the multifunctional coordination sites, involving both nitrogen atoms and carboxylate oxygen atoms, may generate multidimensional structures; (ii) it can be deprotonated to H_2L^-, HL^{2-} and L^{3-}, providing more coordination modes.[21] Fortunately, by exploiting this ligand a novel 3D racemic compound **5** was obtained, in which three kinds of clusters coexist.

Description of crystal structures

***Figure 1** here*

Fig. 1 (a) The 0D cluster in **1**; (b) topological representation of the **pcu** net in **1**, with the $[Fe(1,10\text{-phen})_3]^{2+}$ complexes labeled.

Single crystal X-ray diffraction reveals that compound **1** belongs to the *Pc* space group and its structure features a 0D cluster with the asymmetric unit containing one $[Pr_4Sb_{12}O_{18}Cl_{14.6}(OH)_{2.4}]^{5-}$ cluster, one $Hsal^-$ anion, two $[Fe(1,10\text{-phen})_3]^{2+}$ complexes, two protonated $[2\text{-MepyH}]^+$ groups, and one water guest molecule. As shown in Fig. 1a, compared to the previously reported discrete $[Pr_4Sb_{12}O_{18}Cl_{17}]^{5-}$ cluster containing 12 terminal Cl^- ions (each Pr^{3+} attaches to three Cl^-),[4b] now the COO^- from $Hsal^-$ ligand substituted one terminal Cl^- and

coordinated to Pr(4) in a monodentate fashion. Notably, the phenolic hydroxyl H atom of H_2sal is not deprotonated in **1**, which is common in the previously reported coordination networks.[19a, 19c] Moreover, one of the terminal Cl^- binding Pr(3) is replaced by one OH^- group; while the terminal Cl(6)$^-$ attached to Pr(2) is disordered with a OH^-(O19) group with the occupancy of 0.711(7)/0.289(7), respectively. If each discrete cluster is simplified to a node, the structure of compound **1** can be topologically represented as a α-Po (**pcu**) network (Fig. 1b) by connecting the adjacent nodes. There are two set of $[Fe(1,10\text{-phen})_3]^{2+}$ complexes located in each channel enclosed by the discrete clusters (Fig. 1b).

***Figure 2** here*

Fig. 2 (a) The A cluster in **2**; (b) the B cluster in **2**; (c) prospective view of the 1D anionic structure of **2** along the a-axis, with the $[Fe(3)(1,10\text{-phen})_3]^{2+}$ labeled; top (d) and side (e) view of the simplified nanotubular structure of **2**.

Compound **2** crystallizes in the monoclinic space group $P2_1/c$. The crystallographic asymmetric unit of **2** consists of one formula unit. It is noteworthy that in the asymmetric unit, a carboxyphenoxy group in one of the two types of $bcpb^{3-}$ ligands is disordered over two positions with equal occupancy. As a result, there exist two types of anionic structures in **2** (Fig. S1 in the Supporting Information). One is that the Pr(8) bonds to terminal Cl(24) ion as well as one COO^- group in a chelating mode and meanwhile one dissociating OH^-(O(53)) group near Pr(8) is found to maintain charge balance, resulting in an anionic formula of $\{[Pr_4Sb_{12}O_{18}Cl_{13.5}(OH)_{0.5}](bcpb)_2[Pr_4Sb_{12}O_{18}Cl_{13}(OH)]\}^{10-}$; and the other is that the Pr(8) is coordinated to terminal Cl(23) and Cl(24) ions and one COO^- group in a monodentate mode, giving rise to an anionic formula of $\{[Pr_4Sb_{12}O_{18}Cl_{13.5}(OH)_{0.5}](bcpb)_2[Pr_4Sb_{12}O_{18}Cl_{14}]\}^{10-}$. As a representative example, the crystal structure of the former is described here in detail. As shown in Figs. 2a and 2b, there exist two types of clusters in compound **2** (denoted as A and B clusters, respectively). Compared to the discrete cluster $[Pr_4Sb_{12}O_{18}Cl_{17}]^{5-}$, in A cluster now three COO^- groups from three $bcpb^{3-}$ ligands substitute the three terminal Cl^- ions attached to two Pr^{3+} ions, resulting in a distinct cluster $[(Pr_4Sb_{12}O_{18}Cl_{13.5}(OH)_{0.5})(COO)_3]^{5-}$; while in B cluster three COO^- groups from three $bcpb^{3-}$ ligands substitute the four terminal Cl^- ions attached to three Pr^{3+} ions, resulting in a cluster $[Pr_4Sb_{12}O_{18}Cl_{13}(OH)(COO)_3]^{5-}$. Whereas the remaining one Pr^{3+} (Pr(2) in A cluster or Pr(6) in B cluster) is still coordinated to three Cl^- ions. Also note that another one terminal Cl^- attaching to the Pr(3) in A cluster is disordered with a OH^- group with equal occupancy.

The most intriguing feature of compound **2** is that there exist discrete 1D coordination nanotubes formed by the interconnection of A and B clusters by the $bcpb^{3-}$ ligand. As is well known, the appropriate choice of an organic ligand with specific functional groups and geometry is a major factor in achieving some unique nanotubular structures. Remarkably, in **2** the flexible triangular $bcpb^{3-}$ ligands adopt two kinds of conformations with different coordinating modes: bis-monodentate and bidentate chelating (κ^1)-(κ^1)-$(\kappa^1$-$\kappa^1)$-μ_3 modes, as well as tri-monodentate (κ^1)-(κ^1)-(κ^1)-μ_3 (Types 2-a and 2-b in Scheme 1 and Table 2); the former link adjacent A and B clusters to form a zigzag-like chain, two of which are further joined together by the latter to result in a nanotubular structure along the *a*-axis (Figs. 2c and S2). Overall, the A, B clusters and $bcpb^{3-}$ ligands act as 3-connected nodes. The 1D nanotube of **2** can be simplified as a uninodal net with the point symbol of $\{6^3\}3$ and has a large cross section with a dimension of 20.1 × 13.8 Å (Figs. 2d and 2e). As shown in Fig. 2c, only the $[Fe(3)(1,10\text{-phen})_3]^{2+}$ complexes are located in the interiors of the nanotubes, whereas other three $[Fe(1,10\text{-phen})_3]^{2+}$ and $[2\text{-MepyH}]^+$ are situated between the nanotubular structures.

***Figure 3** here*

Fig. 3 (a) The anionic cluster in **3**; (b) left: prospective view of the 2D layer along the *a*-axis; right: the alternating left-handed (L) and right-handed helical chains (R) in **3**; (c) topological representation of the **fes** net in **3**. In (b), right: all the Sb, O, Cl (except for the central Cl) and Pr(2) atoms in the clusters are omitted for clarity.

Compound **3** crystallizes in the space group $P2_1/n$ and its asymmetric unit consists of one $[Pr_4Sb_{12}O_{18}Cl_{13}(H_2O)_2]^-$ cluster, one $bcpb^{3-}$ ligand, one $[Fe(1,10\text{-phen})_3]^{2+}$ complex, three water guest molecules, as well as two protonated $[3\text{-MepyH}]^+$ groups and two 3-Mepy molecules. As shown in Fig. 3a, compared to the discrete $[Pr_4Sb_{12}O_{18}Cl_{17}]^{5-}$ cluster, now three terminal Cl^- from three Pr^{3+} ions in **3** are substituted by three COO^- groups from three $bcpb^{3-}$ ligands; whereas two other terminal Cl^- attaching to Pr(2) and Pr(3) are replaced by two H_2O molecules, respectively. The $bcpb^{3-}$ acting as tri-monodentate ligand in **3** bridges adjacent clusters to form a highly undulated 2D monolayer on the *bc* plane, consisted of two- and four-membered rings (Fig. 3b, left). Topologically, if each cluster and $bcpb^{3-}$ ligand act as 3–connected nodes, respectively, this 2D sheet can be simplified to a **fes** net (Fig. 3c). It is interesting to note that alternating left-handed and right-handed helical chains are in an orderly arrangement within the 2D sheet, resulting in an achiral structure (Fig. 3b, right). The helical structure may be attributed to the stereoscopic geometry of the bridging $bcpb^{3-}$ ligand.

***Figure 4** here*

Fig. 4 (a) The anionic cluster in **4**; (b) left: prospective view of the 2D double-layer along the *a*-axis, with the $[Fe(1)(1,10\text{-phen})_3]^{2+}$ labeled; right: view of the single-layer along the *c*-axis; (c) schematic representation of the (3,3,6)-connected topological network.

X-ray analysis reveals that compound **4** crystallizes in the space group *P*-1, and its asymmetric unit contains one $[Pr_4Sb_{12}O_{18}Cl_{10}(H_2O)_2]^{2+}$ cluster, two $bcpb^{3-}$ ligands, two $[Fe(1,10\text{-phen})_3]^{2+}$ complexes, three 3-Mepy and thirteen lattice water molecules. Compared to the discrete $[Pr_4Sb_{12}O_{18}Cl_{17}]^{5-}$ cluster, now six terminal Cl^- ions bonded to three Pr^{3+} are substituted by six COO^- groups from six $bcpb^{3-}$ ligands; one termianl Cl^- attaching to Pr(1) is substituted by one H_2O molecule; whereas another terminal Cl^- binding Pr(3) is disordered with a H_2O molecule with equal occupancy (Fig. 4a). Two types of $bcpb^{3-}$ ligands in **4** adopt tri-monodentate coordination modes (Types 4-a and 4-b in Scheme 1 and Table 2), but the roles of them are obviously different during the construction of compound **4**. The former (Type 4-a) bridge adjacent clusters to form a 2D monolayer extending along the *ab* plane (Fig. 4b, right); while the latter (Type 4-b) further connect

two adjacent monolayers to generate a double-layered structure characterized by 1D four-membered ring-like channels along the *a*-axis (Fig. 4b, left). The two independent $[Fe(1,10\text{-phen})_3]^{2+}$ complexes are located in different spaces in compound **4**. The $[Fe(1)(1,10\text{-phen})_3]^{2+}$ occupy the 1D channels, whereas the $[Fe(2)(1,10\text{-phen})_3]^{2+}$ are situated in the interlayer spaces. The 3-Mepy and water guest molecules fill in the rest volumes in compound **4**. From the topological point of view, if the clusters and $bcpb^{3-}$ ligands act as 6-connected and 3-connected nodes, respectively, the 2D double-layer can be viewed as an unprecedented (3,3,6)-connected 3-nodal network with a Schläfli symbol of $\{4.6^2\}\{4^3\}\{4^4.6^8.8^3\}$ analyzed by the Topos 4.0 program (Fig. 4c).[22]

Noticeably, although compounds **3** and **4** were simultaneously obtained through the same solvothermal reaction, their structures show remarkable differences, that are mono-layered structure for **3** and double-layered structure for **4**, which shall be resulted in by the conformational differences of $bcpb^{3-}$ ligands. Considering that hydro(solvo)thermal synthesis is a complex thermodynamic and/or kinetic control process and the subtle variation of assembly environments maybe have a great influence on the crystal nucleation and growth, it is easy to understand the above results. But the above results also inspire us to prepare the compound **3** or **4**, separately; currently, this work is in progress. Also, note that only half of the 3-Mepy in compound **3** are protonated, while the 3-Mepy in compound **4** are all neutral molecules, which can be well proved through TGA-MS analyses (Fig. S3).

***Figure 5** here*

Fig. 5 (a-c) The C, D and E clusters, respectively, in **5**; (d) the coordination modes of the $Hpdc^{2-}$/pdc^{3-} ligands. Color codes: N atoms (blue), H atoms (green). All of the Sb, O, Cl and H atoms (except for O atoms from the COO^- groups, the central Cl atoms and the H atoms bonded to N atoms) in the clusters are omitted for clarity. (e) the connection modes of the clusters shown schematically. The clusters and the H_3pdc ligands are simplified as nodes and linkers, respectively.

Compound **5** belongs to $I4_1/a$ space group, the large unit cell volume of which is comparable to that of protein structures. Its structure features a 3D two-fold interpenetrating racemate which simultaneously contains three kinds of clusters (denoted as C, D and E clusters, respectively). The crystallographic asymmetric unit of **5** consists of half the formula unit. Notably, six crystallographically independent H_3pdc ligands in compound **5** are deprotonated to two different types: $Hpdc^{2-}$ and pdc^{3-} with the ratio of 5:1 (Figs. 5d and S4). The clusters C, D and E can be regarded as the derivatives of the reported discrete cluster $[Pr_4Sb_{12}O_{18}Cl_{17}]^{5-}$ with different amounts of Cl^- ions substituted. In C cluster, now six COO^- groups from four $Hpdc^{2-}$ ligands and two pdc^{3-} ligands substitute the six terminal Cl^- ions attaching to three Pr^{3+} ions, respectively, resulting in a cluster $[Pr_4Sb_{12}O_{18}Cl_9(OH)_2(COO)_6]^{5-}$ (Fig. 5a); in D cluster the eight Cl^- from four Pr^{3+}, respectively, are replaced by eight COO^- from eight $Hpdc^{2-}$ ligands to form a distinct $[Pr_4Sb_{12}O_{18}Cl_9(COO)_8]^{5-}$ cluster (Fig. 5b); while in E cluster two COO^- groups from two different $Hpdc^{2-}$ ligands substitute the two terminal Cl^- ions from a Pr^{3+} ion to give rise to a cluster $[Pr_4Sb_{12}O_{18}Cl_{13}(OH)_2(COO)_2]^{5-}$ (Fig. 5c). As shown in Fig. 5d, all the $Hpdc^{2-}$ and pdc^{3-} ligands in compound **5** act as μ_2-linkers with two monodentate carboxylate groups linking neighboring clusters. It is noteworthy that both the nitrogen atoms in the pyrazole ring do not take part in coordination. Generally, the H_3pdc ligands coordinate to metal centers with both nitrogen and carboxylate oxygen atoms at the same time; by contrast, it is quite rare that the H_3pdc ligands in the same structure all adopt bidentate coordination modes with two carboxylate groups only.[23] Each of the C clusters in compound **5** is linked to two nearest C clusters through two $Hpdc^{3-}$/pdc^{3-} bridges, and one nearest D cluster through a double $Hpdc^{3-}$ bridge; while each of the D clusters is connected to two adjacent C clusters and two E clusters through four double $Hpdc^{3-}$ bridges, respectively; moreover, each of the E cluster acting as a terminal cluster is attached to one D cluster through one double $Hpdc^{3-}$ bridge. The connection fashions of the clusters are clearly illustrated in Fig. 5e. This is highly unusual, considering that the overall framework simultaneously involves three kinds of clusters which are surrounded by as many as 16 ligands.

***Figure 6** here*

Fig. 6 (a) and (b) are the mirror–image representations of the 3D homochiral frameworks with single–stranded four-fold helical chains along the *c*-axis in compound **5**; (c) left: the achiral 2-fold interpenetrating framework of compound **5**; right: the simplified 2-fold interpenetrating framework of **5**. The clusters and ligands are simplified as nodes and linkers, respectively; (d) left: the topological view of the two-fold interpenetrating nets of compound **5**; right: view of the mode of interpenetration observed in **5**.

Significantly, the clusters C and D are firstly connected together by the bridging ligands to form a homochiral 3D framework (Figs. 6a and 6b) with four-fold helices. And then both the 3D frameworks with opposite chirality are interpenetrated to result in the racemic compound **5** crystallizing in the centrosymmetric space group (Fig. 6c). As is known to all, when the enantiomer mixtures aggregate and crystallize, they can form a conglomerate, a racemic solid solution, or a racemic compound in which an even ratio of both enantiomers are present in the same condensate.[24] The above three categories have been widely studied in organic chemistry but got less attention and concern in inorganic–organic hybrid materials. In particular, the 3D hybrid racemic compound is extremely rare to date.[25] As a representative example, one of the 3D homochiral structures, as shown in Fig. 6a, is described here in detail. Two kinds of channels exist along the *c*-axis. The smaller channels are defined by the single-stranded helical chains with the same left-handed chirality formed by the ligands bridging C clusters only. Furthermore, four D clusters connect four such helical chains through $Hpdc^{2-}$ ligands to result in the larger channels (39.9 × 39.9 Å, by measuring the distance of μ_4-Cl^- located in the center of cluster). Significantly, the interior of larger channels are further decorated with the E clusters which attach to D clusters through double $Hpdc^{3-}$ bridges. The five independent $[Fe(1,10\text{-phen})_3]^{2+}$ complexes reside in different spaces of the channels (Fig. S5): the $[Fe(1)(1,10\text{-phen})_3]^{2+}$ are located in the chiral channels, whereas other $[Fe(1,10\text{-phen})_3]^{2+}$ all fill in the larger achiral channels. The $[2\text{-MepyH}]^+$ cations and lattice water molecules fill in both kinds of the channels. After the removal of all the water guest molecules in the channels, the effective solvent accessible volume occupies 18.6% of the total cell volume, calculated using the PLATON program.[17] However,

these counter cations and guest molecules are still not sufficient enough to fill the whole free spaces; so a second network of the same type but opposite chirality interpenetrates the former one in order to stabilize the framework and minimize the big void cavities. From the viewpoint of structural topology, the single 3D framework in **5** can be represented as a (10,3)-a network with a $SrSi_2$ (**srs**) topology by reducing each C cluster as a 3-connected node, which further incorporate with another network having opposite chirality to give a 2-fold interpenetrating framework (Fig. 6d).

From the above structural analyses, we can see clearly that, although the Pr_4Sb_{12} core of the $[Pr_4Sb_{12}O_{18}Cl_{17}]^{5-}$ cluster remains the same, the terminal Cl^- ions attached to the Pr^{3+} ions of the cluster could be substituted by the COO^- and OH^- groups (or H_2O molecules) in different extent to result in different cluster–based units in the compounds **1**–**5**, which were further decorated or interlinked by the organic ligands to form the final structures.

Optical Property

The optical absorption spectra for compounds **1**–**5** were converted from the diffuse reflectance data by using the Kubelka-Munk function.[26] As shown in Fig. 7, the spectra of **1**−**5** are similar and can be assigned to two parts. Compared to the known absorption spectra of $[Fe(1,10\text{-phen})_3]Cl_2$ and the Pr–Sb–O–Cl cluster–based hybrid compounds without $[Fe(1,10\text{-phen})_3]^{2+}$ counter ion,[4b, 27] the intense absorption bands at about 2.4 eV for **1**–**5** arise from the metal to ligand charge transfer (MLCT) of

***Figure 7** here*

Fig. 7. Solid–state optical absorption spectra of compounds **1**–**5**.

$[Fe(1,10\text{-phen})_3]^{2+}$; and the broad bands in the area larger than about 4.0 eV for **1**–**5** are assigned to cluster–centered bands overlapped with $\pi\cdots\pi^*$ transitions of the 1,10-phen ligand. From the given absorption edges of the intense MLCT bands, the band gaps of **1**–**5** can be estimated to be 2.07, 2.04, 2.11, 2.06 and 2.08 eV, respectively, which are consistent with their colors. Compared to other cluster–based compounds integrated with a metal complex of 1,10-phen,[27] the cation–anion charge-transfer band (CACT) between both the absorption bands above in compunds **1**–**5** is not observed, due to the weaker intermolecular interactions (such as hydrogen bonds and/or $\pi\cdots\pi$ interactions) between the metal complex cations and the anionic framework.

***Figure 8** here*

Fig. 8 Time course of H_2 evolution from Pt-loaded photocatalyst **3** (50 mg, 3 wt% Pt) under UV–light irradiation using a 300 W Xe lamp in 100 mL of 10% CH_3OH aqueous solution.

Hydrogen Evolution

To demonstrate the potential use of compound **3** as a photocatalyst, photocatalytic hydrogen evolution was performed under UV–light radiation (λ > 300 nm) in 100 mL 10% CH_3OH solution containing 50 mg compound **3** as a catalyst, and 3 wt% Pt was in–situ loaded on the surface of the catalyst as co-catalyst. As shown in Fig. 8, H_2 continuously evolved with the duration of UV–light irradiation. A total amount of 0.50 μmol H_2 was generated after 5h, which was comparable to that of another Pr–Sb–O–Cl clusters–based compound reported by us previously.[4c] The blank reaction (without compound **3** as a catalyst) was also carried out, and even after 10h sustained irradiation the produced H_2 was no more than 0.2 μmol, which strongly demonstrates the excellent photochemistry activity of the compound **3** in solid–liquid solution under UV–light radiation. Significantly, compound **3** possesses an enhanced UV–light photocatalytic activity in comparison with the reported POMs.[28]

***Figure 9** here*

Fig. 9 Temperature dependence of $\chi_m T$ *vs* *T* curves for **1** and **5** under an applied field of 1000 Oe in the temperature range of 2–300 K, respectively.

Magnetic Properties

The temperature–dependent magnetic susceptibilities of **1** and **5** were carried out under a magnetic field of 1000 Oe in the temperature range of 2–300 K, respectively. As shown in Fig. 9, both compounds exhibit similar magnetic behaviors. At 300 K, the observed $\chi_m T$ values for compounds **1** and **5** were 6.49 $cm^3\cdot K\cdot mol^{-1}$ and 28.57 $cm^3\cdot K\cdot mol^{-1}$, respectively. As the temperature was lowered, the $\chi_m T$ values decreased smoothly and reached 0.43 $cm^3\cdot K\cdot mol^{-1}$ for compound **1** and 2.87 $cm^3\cdot K\cdot mol^{-1}$ for compound **5** at 2 K. The magnetic susceptibility data of **1** above 15 K (10 K for **5**) follow the Curie–Weiss law well, giving Curie and Weiss constants of C = 6.94 $cm^3\cdot K\cdot mol^{-1}$, θ = -28.31 K for compound **1** and C = 30.48 $cm^3\cdot K\cdot mol^{-1}$, θ = -17.61 K for compound **5**, respectively (Fig. S6). The decrease of the $\chi_m T$ value with decreasing temperature and a negative value of θ suggest an antiferromagnetic interaction in compound **1** or **5**.

Conclusions

A series of Pr–Sb–O–Cl clusters–based compounds, from discrete cluster to 3D inorganic–organic hybrid framework, have been synthesized and structurally characterized. The successful syntheses of compounds **1**–**5** not only demonstrate that solvent, ligand, reaction temperature and time effects on the structures, but also offer guidance for the design and synthesis of novel clusters–based hybrid structures. The differently structural and topological motifs of compounds **2**–**4** demonstrate that the flexible H_3bcpb ligand is an excellent structural contributor for hybrid frameworks. A photocatalytic investigation indicated that compound **3** was active for photocatalytic H_2 evolution under UV–light irradiation, which further highlights that the hybrid lanthanide–antimony–oxohalide cluster–based compounds as catalysts are good candidates for photocatalytic H_2 evolution. Least but not last, next it is hoped to obtain a conglomerate rather than the racemic compound **5** by further adjusting the reaction conditions and ultimately achieve spontaneous resolution.

Acknowledgements

This work was supported by the 973 program (2012CB821702) and by the NNSF of China (21221001).

Notes and references

[a] *State Key Laboratory of Structural Chemistry, Fujian Institute of Research on the Structure of Matter, the Chinese Academy of Sciences, Fuzhou, Fujian 350002, P.R. China. Fax: (+86) 591-83793727; Tel: (+86) 591-83793727; E-mail: xyhuang@fjirsm.ac.cn*

[b] *University of Chinese Academy of Sciences, Beijing, 100049, P.R. China*

[c] College of Chemistry and Chemical Engineering, Fuzhou University, Fuzhou, Fujian, 350002, P.R. China

† Electronic Supplementary Information (ESI) available: X-ray crystallographic files in CIF format, more structure figures, additional magnetic data, experimental and simulated X-ray powder patterns, TGA and TGA-MS data. CCDC 976937-976941. For ESI and crystallographic data in CIF or other electronic format, see DOI: 10.1039/b000000x/

1 (a) S. T. Zheng, G. Y. Yang, *Chem. Soc. Rev.* 2012, **41**, 7623; (b) D.-L. Long, R. Tsunashima, L. Cronin, *Angew. Chem., Int. Ed.* 2010, **49**, 1736; (c) G. E. Kostakis, S. P. Perlepes, V. A. Blatov, D. M. Proserpio, A. K. Powell, *Coord. Chem. Rev.* 2012, **256**, 1246; (d) P. Vaqueiro, M. L. Romero, *J. Am. Chem. Soc.* 2008, **130**, 9630.

2 (a) U. Schubert, *Chem. Soc. Rev.* 2011, **40**, 575; (b) A. Dolbecq, E. Dumas, C. R. Mayer, P. Mialane, *Chem. Rev.* 2010, **110**, 6009.

3 (a) T. Wu, R. Khazhakyan, L. Wang, X. H. Bu, S. T. Zheng, V. Chau, P. Y. Feng, *Angew. Chem., Int. Ed.* 2011, **50**, 2536; (b) P. Vaqueiro, M. L. Romero, B. C. Rowan, B. S. Richards, *Chem. Eur. J.* 2010, **16**, 4462.

4 (a) B. Hu, G.-D. Zou, M.-L. Feng, X.-Y. Huang, *Dalton Trans.* 2012, **41**, 9879; (b) B. Hu, M.-L. Feng, J.-R. Li, Q.-P. Lin, X.-Y. Huang, *Angew. Chem., Int. Ed.* 2011, **50**, 8110; (c) G.-D. Zou, G.-G. Zhang, B. Hu, J.-R. Li, M.-L. Feng, X.-C. Wang, X.-Y. Huang, *Chem. Eur. J.* 2013, **19**, 15396.

5 S. Iijima, *Nature*. 1991, **354**, 56.

6 (a) K. Suenaga, C. Colliex, N. Demoncy, A. Loiseau, H. Pascard, F. Willaime, *Science*. 1997, **278**, 653; (b) W. Tremel, *Angew. Chem., Int. Ed.* 1999, **38**, 2175; (c) D. Tasis, N. Tagmatarchis, A. Bianco, M. Prato, *Chem. Rev.* 2006, **106**, 1105.

7 (a) M. R. Ghadiri, J. R. Granja, R. A. Milligan, D. E. McRee, N. Khazanovich, *Nature*. 1994, **372**, 709; (b) R. Chapman, M. Danial, M. L. Koh, K. A. Jolliffe, S. Perrier, *Chem. Soc. Rev.* 2012, **41**, 6023; (c) J. West, A. Manz, P. S. Dittrich, *Langmuir*. 2008, **24**, 6754.

8 (a) W. Xiong, F. Du, Y. Liu, A. Perez, Jr., M. Supp, T. S. Ramakrishnan, L. Dai, L. Jiang, *J. Am. Chem. Soc.* 2010, **132**, 15839; (b) S. Hao, G. Zhou, W. Duan, J. Wu, B.-L. Gu, *J. Am. Chem. Soc.* 2008, **130**, 5257; (c) V. Sgobba, D. M. Guldi, *Chem. Soc. Rev.* 2009, **38**, 165; (d) V. G. Organo, D. M. Rudkevich, *Chem. Commun.* 2007, 3891; (e) M. A. B. Block, S. Hecht, *Angew. Chem., Int. Ed.* 2005, **44**, 6986.

9 (a) H. Furukawa, K. E. Cordova, M. O'Keeffe, O. M. Yaghi, *Science*. 2013, **341**, 974; (b) K. Sumida, D. L. Rogow, J. A. Mason, T. M. McDonald, E. D. Bloch, Z. R. Herm, T.-H. Bae, J. R. Long, *Chem. Rev.* 2012, **112**, 724; (c) M. P. Suh, H. J. Park, T. K. Prasad, D.-W. Lim, *Chem. Rev.* 2012, **112**, 782; (d) J.-R. Li, J. Sculley, H.-C. Zhou, *Chemical Reviews*. 2012, **112**, 869; (e) E. Coronado, G. Minguez Espallargas, *Chem. Soc. Rev.* 2013, **42**, 1525.

10 (a) X.-C. Huang, W. Luo, Y.-F. Shen, X.-J. Lin, D. Li, *Chem. Commun.* 2008, 3995; (b) P. Thanasekaran, T.-T. Luo, C.-H. Lee, K.-L. Lu, *J. Mater. Chem.* 2011, **21**, 13140; (c) D. K. Unruh, K. Gojdas, A. Libo, T. Z. Forbes, *J. Am. Chem. Soc.* 2013, **135**, 7398; (d) Z.-Z. Lu, R. Zhang, Y.-Z. Li, Z.-J. Guo, H.-G. Zheng, *J. Am. Chem. Soc.* 2011, **133**, 4172; (e) O. S. Jung, Y. J. Kim, K. M. Kim, Y. A. Lee, *J. Am. Chem. Soc.* 2002, **124**, 7906.

11 (a) K. Otsubo, Y. Wakabayashi, J. Ohara, S. Yamamoto, H. Matsuzaki, H. Okamoto, K. Nitta, T. Uruga, H. Kitagawa, *Nat. Mater.* 2011, **10**, 291; (b) T. Panda, T. Kundu, R. Banerjee, *Chem. Commun.* 2012, **48**, 5464; (c) F. Dai, H. He, D. Sun, *J. Am. Chem. Soc.* 2008, **130**, 14064; (d) T.-T. Luo, H.-C. Wu, Y.-C. Jao, S.-M. Huang, T.-W. Tseng, Y.-S. Wen, G.-H. Lee, S.-M. Peng, K.-L. Lu, *Angew. Chem., Int. Ed.* 2009, **48**, 9461; (e) Y.-B. Dong, Y.-Y. Jiang, J. Li, J.-P. Ma, F.-L. Liu, B. Tang, R.-Q. Huang, S. R. Batten, *J. Am. Chem. Soc.* 2007, **129**, 4520.

12 A. Fujishima, K. Honda, *Nature*. 1972, **238**, 37.

13 (a) M. Higashi, K. Domen, R. Abe, *J. Am. Chem. Soc.* 2012, **134**, 6968; (b) X. Chen, S. Shen, L. Guo, S. S. Mao, *Chem. Rev.* 2010, **110**, 6503; (c) F. A. Frame, E. C. Carroll, D. S. Larsen, M. Sarahan, N. D. Browning, F. E. Osterloh, *Chem. Commun.* 2008, 2206.

14 (a) W. J. Youngblood, S.-H. A. Lee, K. Maeda, T. E. Mallouk, *Acc. Chem. Res.* 2009, **42**, 1966; (b) A. Kudo, Y. Miseki, *Chem. Soc. Rev.* 2009, **38**, 253; (c) F. E. Osterloh, *Chem. Mater.* 2007, **20**, 35.

15 (a) Z. Y. Zhang, Q. P. Lin, D. Kurunthu, T. Wu, F. Zuo, S. T. Zheng, C. J. Bardeen, X. H. Bu, P. Y. Feng, *J. Am. Chem. Soc.* 2011, **133**, 6934; (b) Z. Y. Zhang, Q. P. Lin, S. T. Zheng, X. H. Bu, P. Y. Feng, *Chem. Commun.* 2011, **47**, 3918; (c) P. Huang, C. Qin, Z.-M. Su, Y. Xing, X.-L. Wang, K.-Z. Shao, Y.-Q. Lan, E.-B. Wang, *J. Am. Chem. Soc.* 2012, **134**, 14004; (d) Z.-L. Wang, H.-Q. Tan, W.-L. Chen, Y.-G. Li, E.-B. Wang, *Dalton Trans.* 2012, **41**, 9882.

16 G. M. Sheldrick, *SHELX 97, Program for Crystal Structure Solution and Refinement, University of Göttingen: Germany*. 1997.

17 P. Vandersluis, A. L. Spek, *Acta Crystallogr. Sect. A*. 1990, **46**, 194.

18 (a) D. Fenske, C. E. Anson, A. Eichhöfer, O. Fuhr, A. Ingendoh, C. Persau, C. Richert, *Angew. Chem., Int. Ed.* 2005, **44**, 5242; (b) S. Chitsaz, D. Fenske, O. Fuhr, *Angew. Chem., Int. Ed.* 2006, **45**, 8055.

19 (a) Y. Yang, P. Du, J. F. Ma, W. Q. Kan, B. Liu, J. Yang, *Cryst. Growth Des.* 2011, **11**, 5540; (b) S. K. Langley, N. F. Chilton, B. Moubaraki, K. S. Murray, *Dalton Trans.* 2011, **40**, 12201; (c) M. Devereux, M. McCann, M. T. Casey, M. Curran, G. Ferguson, C. Cardin, M. Convery, V. Quillet, *J. Chem. Soc.-Dalton Trans.* 1995, 771.

20 (a) J. Cui, Y. Li, Z. Guo, H. Zheng, *Chem. Commun.* 2013, **49**, 555; (b) J. Cui, Y. Li, Z. Guo, H. Zheng, *Cryst. Growth Des.* 2012, **12**, 3610.

21 (a) X. H. Zhou, X. D. Du, G. N. Li, J. L. Zuo, X. Z. You, *Cryst. Growth Des.* 2009, **9**, 4487; (b) J. Xia, B. Zhao, H. S. Wang, W. Shi, Y. Ma, H. B. Song, P. Cheng, D. Z. Liao, S. P. Yan, *Inorg. Chem.* 2007, **46**, 3450; (c) K. C. Stylianou, J. E. Warren, S. Y. Chong, J. Rabone, J. Bacsa, D. Bradshaw, M. J. Rosseinsky, *Chem. Commun.* 2011, **47**, 3389.

22 V. A. Blatov, A. P. Shevchenko, V. N. Serezhkin, *J. Appl. Crystallogr.* 2000, **33**, 1193.

23 L. Pan, T. Frydel, M. B. Sander, X. Y. Huang, J. Li, *Inorg. Chem.* 2001, **40**, 1271.

24 (a) J. Jacques, A. Collet, S. Wilen, *Enantiomers, Racemates and Resolutions*, Krieger Publishing Company, Malabar, Florida, **1994**; (b) L. Perez-Garcia, D. B. Amabilino, *Chem. Soc. Rev.* 2002, **31**, 342.

25 H. He, G.-J. Cao, S.-T. Zheng, G.-Y. Yang, *J. Am. Chem. Soc.* 2009, **131**, 15588.

26 W. W. Wendlandt, H. G. Hecht, *Reflectance Spectroscopy*, Interscience Publishers, New York, **1966**.

27 (a) Z.-X. Lei, Q.-Y. Zhu, X. Zhang, W. Luo, W.-Q. Mu, J. Dai, *Inorg. Chem.* 2010, **49**, 4385; (b) X. Zhang, W. Luo, Y.-P. Zhang, J.-B. Jiang, Q.-Y. Zhu, J. Dai, *Inorg. Chem.* 2011, **50**, 6972.

28 H. Fu, Y. Lu, Z. Wang, C. Liang, Z.-M. Zhang, E. Wang, *Dalton Trans.* 2012, **41**, 4084.

Table 1. Crystallographic data for **1**–**5**.

	1	**2**	**3**	**4**	**5**
Empirical formula	$C_{91}H_{73.4}O_{24.4}N_{14}Cl_{14.6}Fe_2Sb_{12}Pr_4$	$C_{198}H_{219}N_{26}O_{95}Cl_{27}Fe_4Sb_{24}Pr_8$	$C_{81}N_{10}H_{75}O_{31}Cl_{13}FeSb_{12}Pr_4$	$C_{132}N_{15}H_{121}O_{49}Cl_{10}Fe_2Sb_{12}Pr_4$	$C_{456}H_{538}Cl_{53}Fe_{10}N_{90}O_{256}Pr_{20}Sb_{60}$
Formula weight	4407.34	9712.81	4225.85	5192.27	23936.28
Crystal system	monoclinic	monoclinic	monoclinic	triclinic	tetragonal
Space group	*Pc*	$P2_1/c$	$P2_1/n$	*P*-1	$I4_1/a$
a/Å	12.9468(17)	19.9710(3)	12.8307(3)	17.7472(3)	59.1220(7)
b/Å	18.388(2)	22.2647(3)	27.0624(9)	19.1035(3)	59.1220(7)
c/Å	25.369(3)	59.856 (1)	32.2935(7)	24.6190(4)	39.2567(3)
α/°	90	90	90	95.473(1)	90
β/°	97.239(2)	94.997(2)	95.917(2)	91.112(1)	90
γ/°	90	90	90	110.914(2)	90
V/Å^3	5991.4(13)	26513.7(7)	11153.5(5)	7748.4(2)	137218(3)
Z	2	4	4	2	8
T/K	295(2)	100(2)	295(2)	295(2)	100(2)
Flack parameter	0.049(12)				
ρ_{calcd} /g cm^{-3}	2.443	2.433	2.517	2.225	2.317
u/mm^{-1}	4.876	35.022	5.076	3.724	33.345
F(000)	4122	18432	7896	4960	90824
Measured refls.	49294	102603	49890	65391	197391
Independent refls.	21633	47892	22772	31643	62536
No. of parameters	1489	3575	1513	2039	4042
R_{int}	0.0365	0.0532	0.0266	0.0289	0.1024
GOF	1.005	1.093	0.994	1.041	1.246
R_1 ($I > 2\sigma(I)$)	0.0351	0.0858	0.0380	0.0393	0.1379
$wR(F_2)$ ($I > 2\sigma(I)$)	0.0570	0.2053	0.0831	0.0894	0.2414

[a] $R_1 = \sum \| F_o | - | F_c \| / \sum | F_o |$. [b] $wR_2 = [\sum w(F_o^2 - F_c^2)^2 / \sum w(F_o^2)^2]^{1/2}$.

Table 2 Comparison of the corresponding angles (deg) in H_3bcpb ligands among compounds **2**–**4**.

	2-a	**2-b**	**3-a**	**4-a**	**4-b**
angle *α*	119.852(2)	115.845(2)	117.636(3)	120.024(4)	116.659(4)
angle *β*	118.649(2)	117.414(2)	118.620(3)	121.332(2)	120.399(3)
dihedral angle$_{[Cg(I)-Cg(II)]}$	73.132	85.992	89.008	62.009	83.381
dihedral angle$_{[Cg(I)-Cg(III)]}$	79.387	82.924	66.791	67.574	67.907
dihedral angle$_{[Cg(II)-Cg(III)]}$	81.217	73.937	42.430	82.562	79.378

Scheme 1 here

Scheme 1 Different conformations of the flexible triangular bcpb^{3-} ligand in compounds **2** (2-a and 2-b), **3** (3-a) and **4** (4-a and 4-b).

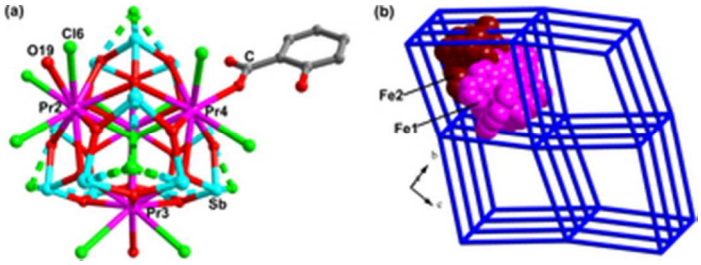

Fig. 1
29x10mm (300 x 300 DPI)

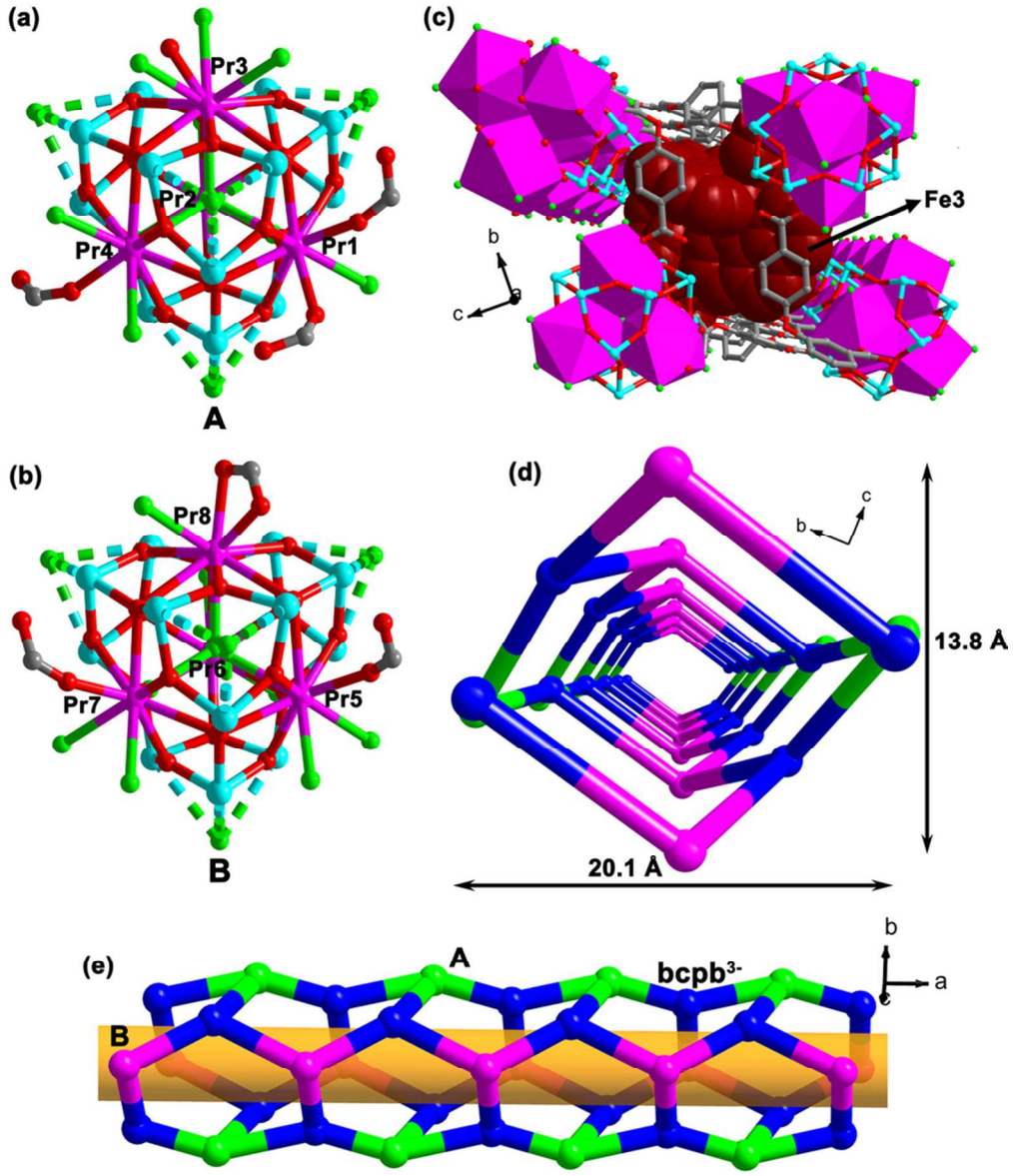

Fig. 2
81x96mm (300 x 300 DPI)

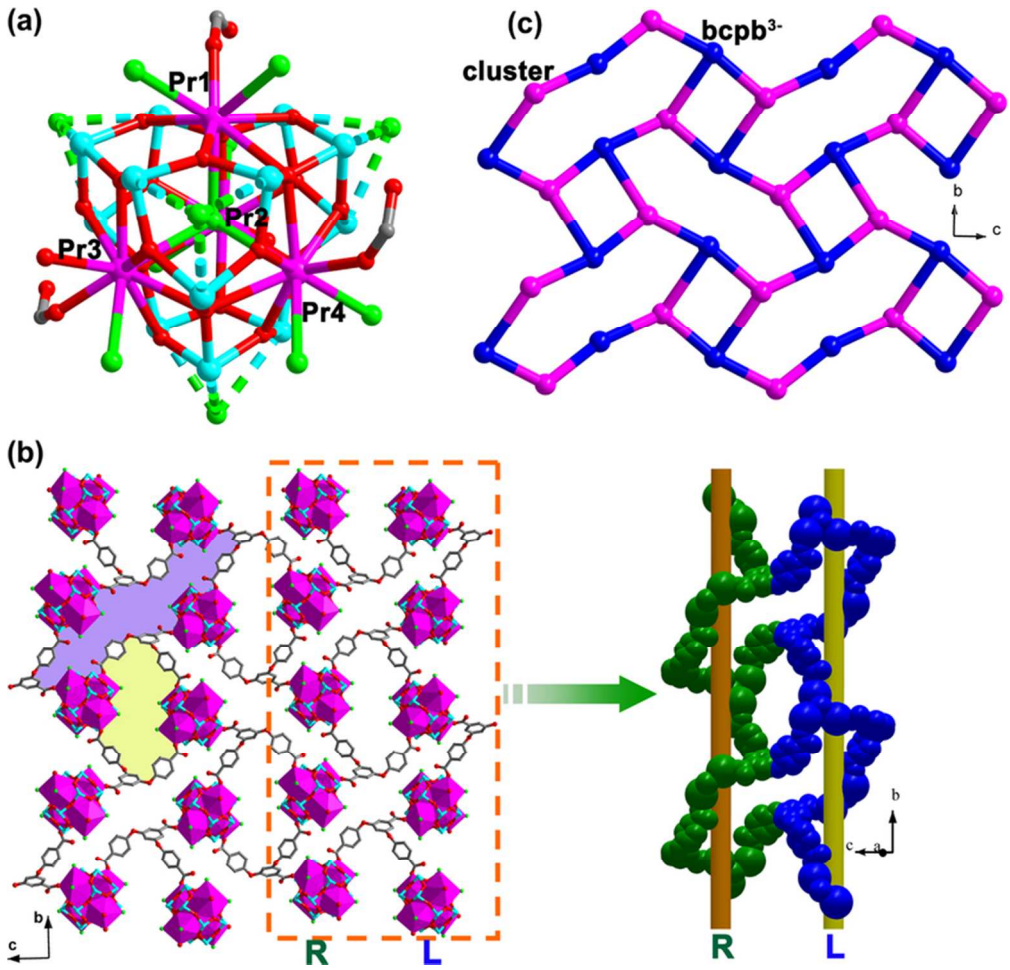

Fig. 3
71x68mm (300 x 300 DPI)

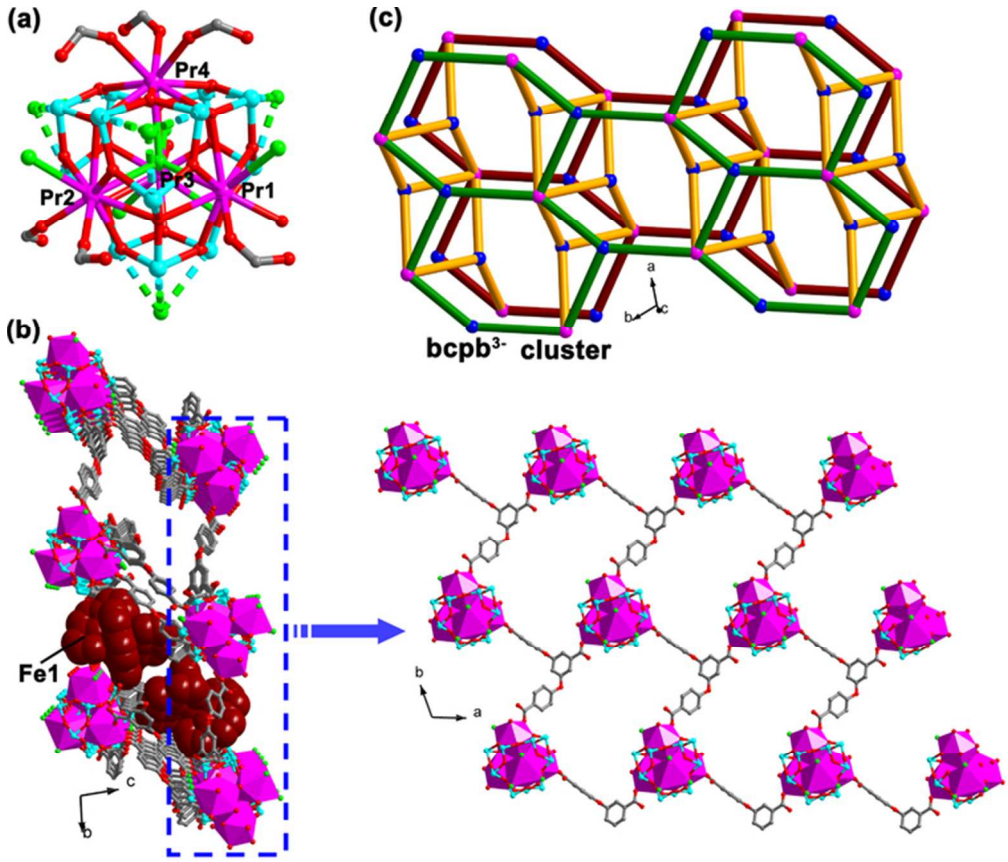

Fig. 4
63x54mm (300 x 300 DPI)

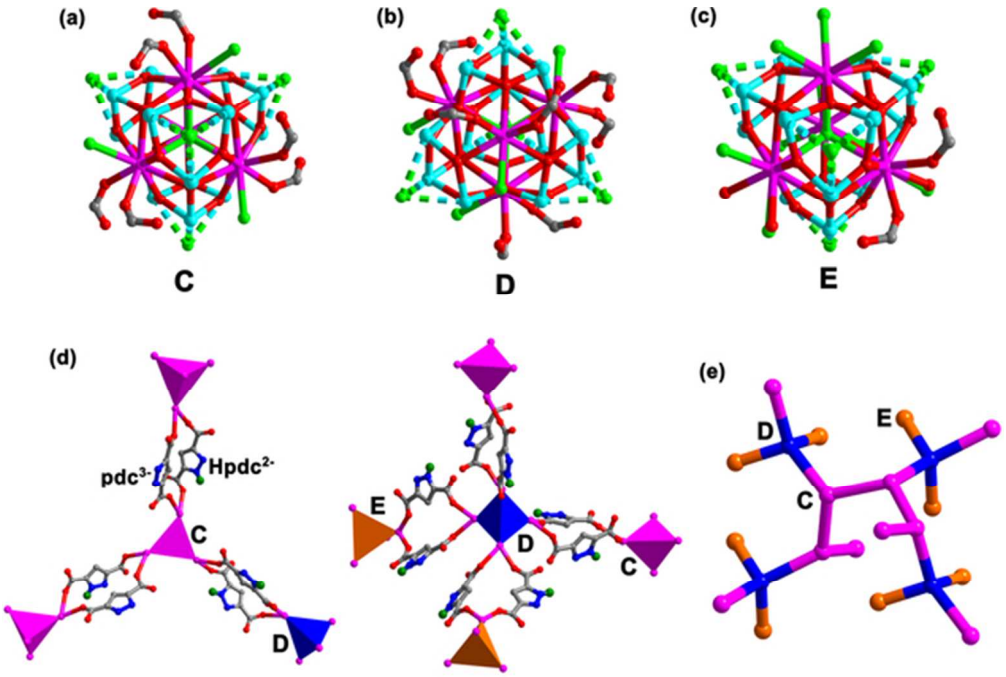

Fig. 5
53x35mm (300 x 300 DPI)

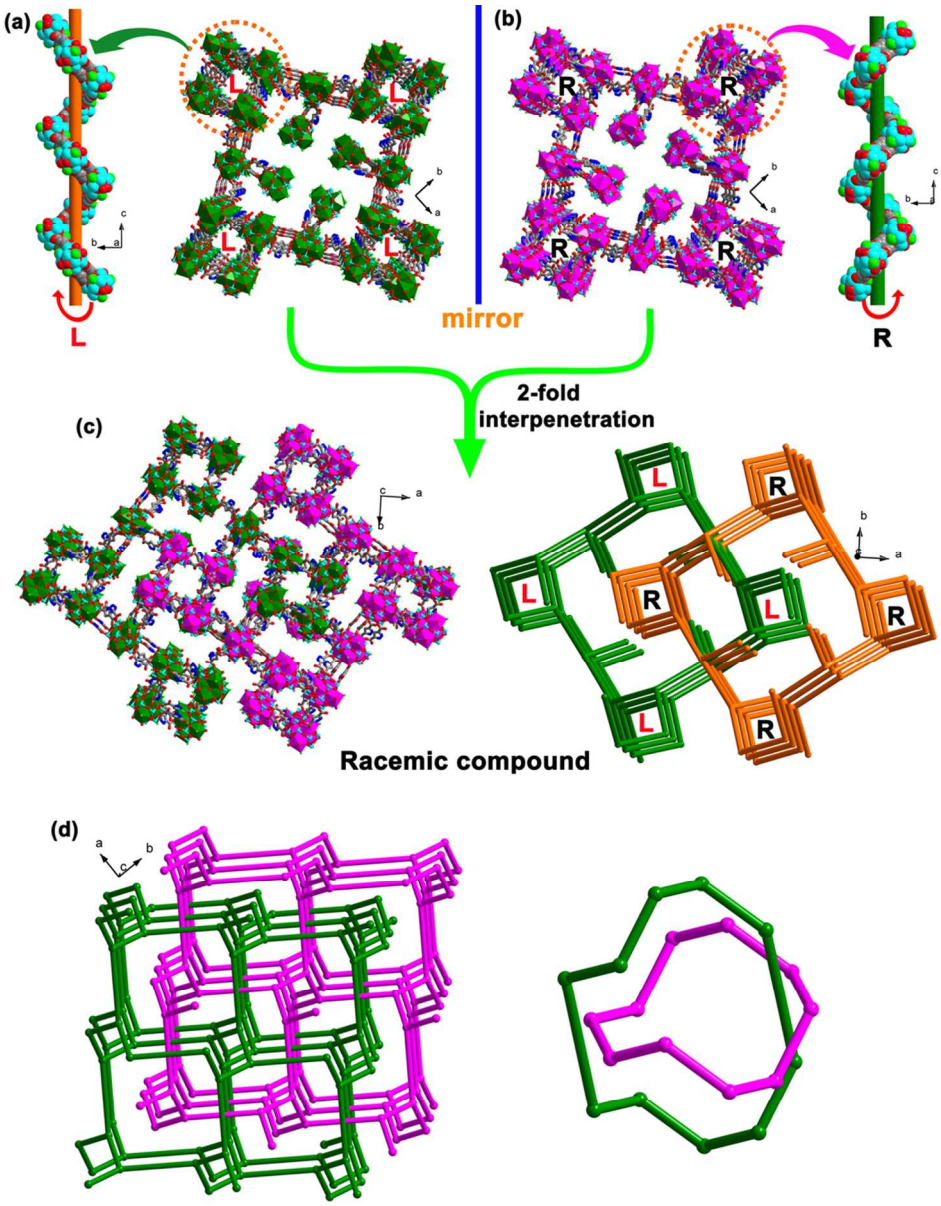

Fig. 6
96x122mm (300 x 300 DPI)

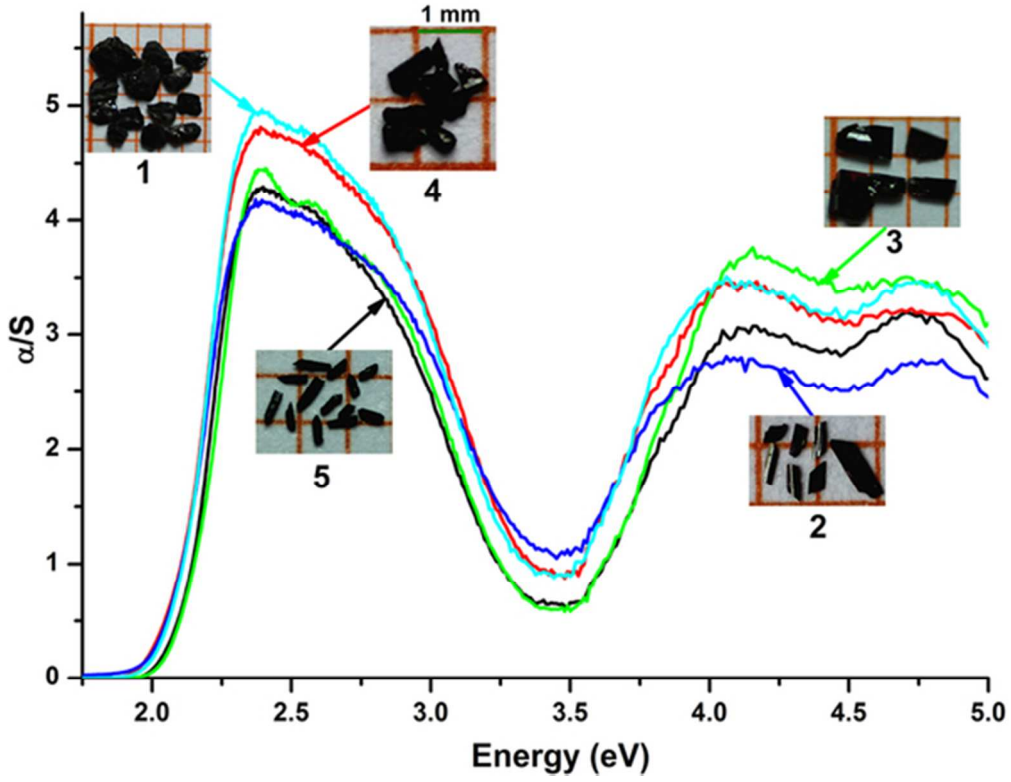

Fig. 7
50x39mm (300 x 300 DPI)

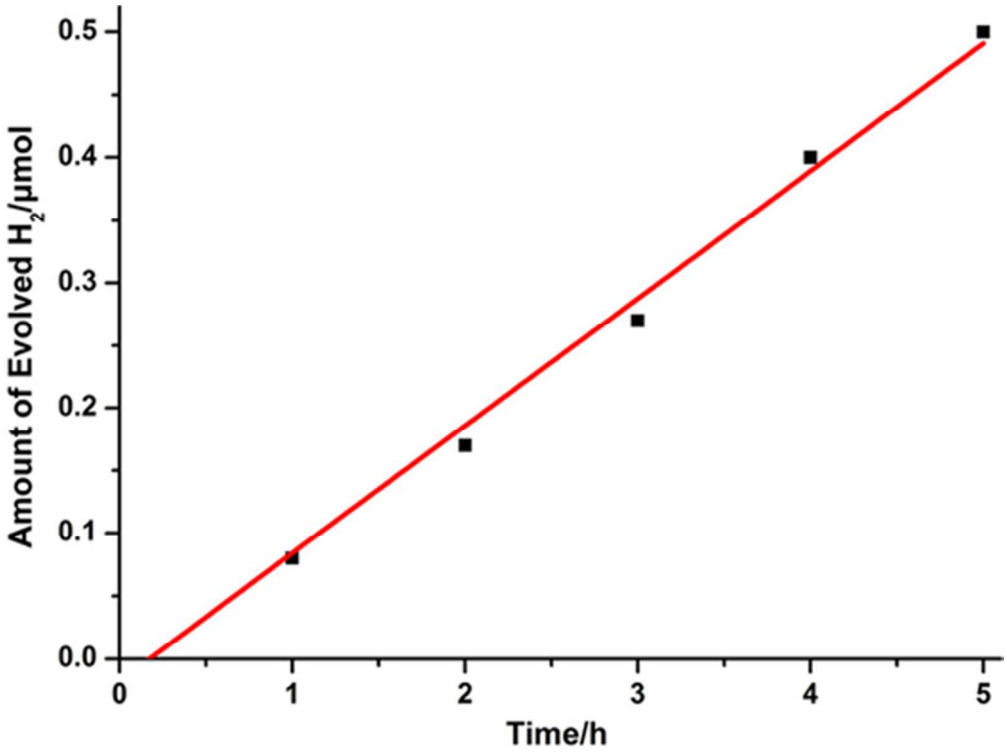

Fig. 8
44x33mm (300 x 300 DPI)

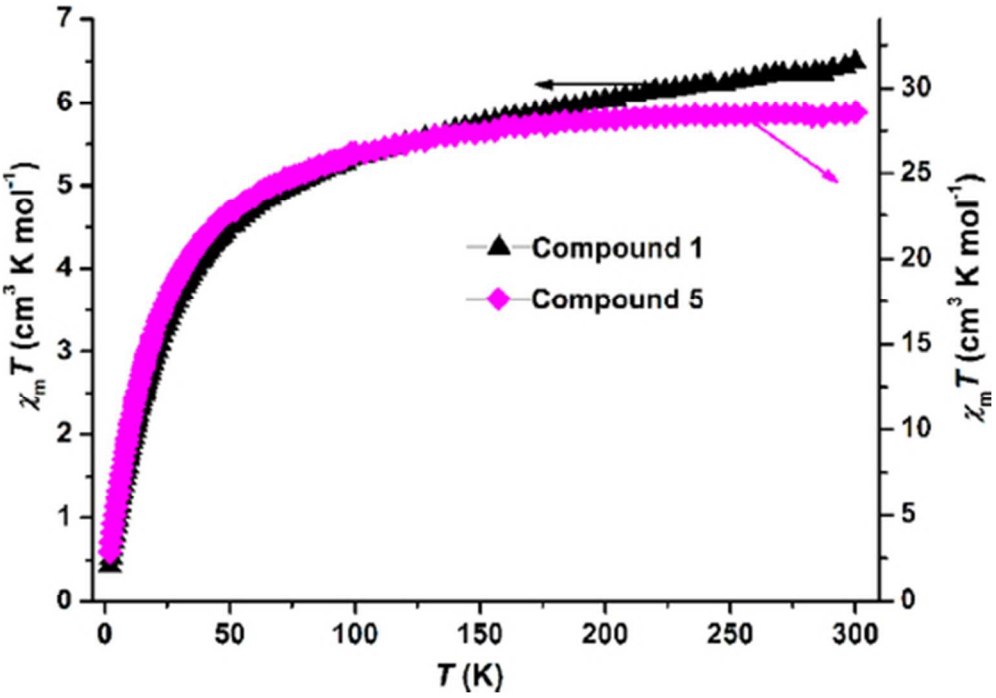

Fig. 9
41x29mm (300 x 300 DPI)

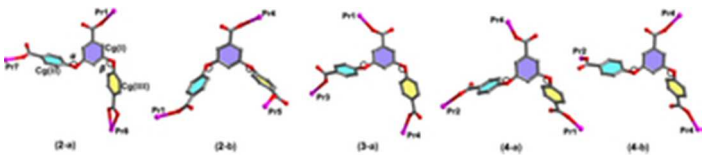

Scheme 1
29x6mm (300 x 300 DPI)

TOC

Syntheses, Structures and Photocatalytic Properties of Five New Praseodymium–Antimony Oxochlorides: From Discrete Cluster to 3D Inorganic–Organic Hybrid Racemic Compound

Guo–Dong Zou, Ze–Ping Wang, Ying Song, Bing Hu and Xiao–Ying Huang*

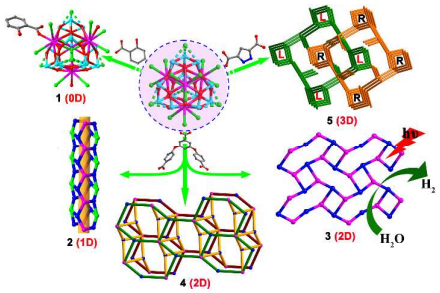

Presented are five Pr–Sb–O–Cl cluster–based compounds containing discrete organic-decorated cluster to 3D hybrid anionic structures and exhibiting photocatalytic H_2-evolution activity and magnetic properties.